Tunnelling and Underground Space Technology 77 (2018) 295–304

Contents lists available at ScienceDirect

Tunnelling and Underground Space Technology

journal homepage: www.elsevier.com/locate/tust

Shaking table tests on seismic response and damage mode of tunnel linings in diverse tunnel-void interaction states

C.L. Xin[a], Z.Z. Wang[b,*], B. Gao[c]

[a] Department of Underground Engineering, Taiyuan University of Technology, Taiyuan, PR China
[b] School of Civil Engineering, Dalian University of Technology, Dalian, PR China
[c] Key Laboratory of Transportation Tunnel Engineering of Ministry of Education, Southwest Jiaotong University, Chengdu, PR China

ARTICLE INFO

Keywords:
Tunnel engineering
Shaking table test
Void-lining interaction
Seismic response

ABSTRACT

The voids between the primary and the secondary linings for tunnel structures can be regarded as the worst contact state, which is deemed as serious tunnel quality defect. Recently, researchers have attempted to study tunnel linings behavior with the voids mostly in static state but these sort of defective tunnel linings are easier to destroy by earthquake. A shaking table-based method to determine the behavior of tunnels subject to the voids behind linings can be the ideal method to study their interaction in seismic dynamic states. This paper presents results from a series shaking table tests on scaled tunnel models with and without the void on the lining crown under increasing seismic intensities excitations. Details of experimental setup and procedures are described first and then the test results are presented. The test results are discussed based on the acceleration amplification factors, tension-compression strains, and damage patterns. The comparison shows that the peak acceleration on the outer surface of lining crown with a void is greater than without a void after inputting the peak ground acceleration (PGA) beyond 0.4 g regardless of the excitation directions. Each monitoring point on lining models without a void is mainly in the reasonable stress state and the most adverse strain state generates on the arch springing. There is nearly no strains difference between lining models in tight and loose contact states while the input PGA grows from 0.2 g to 0.4 g. However, plenty of tension strains appear and increase from the crown to the sidewall of lining model with a void with the input PGA increasing from 0.6 g to 1.0 g. Accordingly, multiple longitudinal cracks along axis of lining model are generated from the crown to the sidewall but three annular cracks on outer surface of lining crown should be focused attention. Finally, it is found that tunnel models behavior with and without voids behind the linings in the shaking table tests compared favorably with that in seismic damage instances.

1. Introduction

Recent series strong earthquakes in China, such as the 2008 Mw 8.0 Wenchuan earthquake, 2013 Mw 7.0 Lushan earthquake and 2017 Mw 7.0 Jiuzhaigou earthquake, had testified the vulnerability of tunnels (Baziar et al, 2014; Moghadam and Baziar, 2016), quite a substantial proportion of which were actually defective during construction or operation periods (Wang et al., 2001, 2009, 2013; Li, 2012; Yu et al., 2016a). One of quality defects is void between secondary lining and surrounding rock (Nie et al., 2015). In reality, void is one of the three types of contact states between secondary lining and surrounding rock for tunnel structures. The other two are tight and loose contact state respectively. Both the loose contact state and the voids behind the lining can be regarded as poor contacts, which are also deemed as typical inducements of other tunnel quality defects (Zhang et al., 2013). Due to the inherent characteristics of concealment and randomness, generally, voids do not directly lead to structural damage in static state but it is related to a large number of compound and secondary tunnel defects. Although voids defects are not difficult to detect, they are not easy to renovate perfectly (Wang et al., 2010). Hence, this type of defects has received minimal attention from the design, construction and operation communities, and much more the earthquake engineering community (Meguid and Dang, 2009; Oreste, 2014). Whereas in seismic state, this lack of attention may stem from the fact that tunnel structures with voids have generally been considered to perform well in small to moderate earthquakes due to their lower constraining forces that lead to limited seismic inertia forces (Leung and Meguid, 2011). However, what has been underestimated is that the constrain effects from surrounding rock, which is directly related to complicate and potential hazards of tunnel structures in earthquakes (Yu and Rowe,

* Corresponding author.
E-mail address: wangzhengzheng@dlut.edu.cn (Z.Z. Wang).

https://doi.org/10.1016/j.tust.2018.03.010
Received 23 August 2017; Received in revised form 23 November 2017; Accepted 6 March 2018

1999; Fraldi and Guarracino, 2009; Jones and Hunt, 2011).

As mentioned above, relatively few studies conducted on seismic responses and damage modes of tunnel structures with voids but the performance of tunnel structures with void to withstand moderate to severe seismic events was still questionable. To address the tunnel-void interaction issue in static and seismic states, many geophysical scientists initiated voids position detection projects by using various non-destructive approaches and techniques (Fang et al., 2016). There was no doubt that the voids behind secondary linings and primary supports were very common especially which were on the outer surfaces of lining crowns, spandrels and sidewalls (Zhou et al., 2017). Furthermore, in many high intensity seismic areas, it is ordinary that the total length of voids between secondary lining and surrounding rock is more than 10% of railway tunnels length or even more than 50% of highway tunnels length (Zhang et al., 2016). Investigation has proven that three main reasons as construction methods, design mistakes and geological conditions can result in voids; meanwhile the results from voids have started to draw attention of researchers (Gao et al., 2014). There are three phases to describe the evolutionary process of void-inducing disasters. First, voids appearances have strong influence on worsening the constrain interaction of linings and rock, especially on squeezing lining structures and loosing surrounding rock (Balkaya et al., 2012). Second, voids expansion is effective in lining cracking or even spalling due to the seepage, unsymmetrical overloading of lining and absent counterforce of rock, thereby leading to reduction of reliability and durability (Huang et al., 2013). Third, voids shrink and collapse are highly beneficial for reducing carrying capacity and serviceable security owing to the superimposition of loose contact states behind primary supports and secondary linings (Wang et al., 2014). Thus, it is important to detect, backfill or grout the voids behind lining in time, especially which are on the tunnel lining crown.

To date, many transport tunnels have been unavoidably constructed in seismic fortification zones and voids concealing areas. Fig. 1 shows the damage patterns of tunnel structures with voids on its crown after Wenchuan Great Earthquake (Wang et al., 2015). Thus, it is of great significance to study the seismic damage mechanism of tunnel linings with voids defects, which is helpful to protect serviceability of transport tunnels under and after earthquake attack. Herein, this research aims to study the seismic response and damage patterns of tunnel linings in diverse tunnel-void interaction states. Thereby we had designed and conducted a series of shaking table tests on lining models with voids on lining crowns. Technical details of the tests including test facilities, experimental setup, soil and lining models, design and fabrication of the soil container and simulations of seismic excitations are presented in this paper. The results obtained in this study may provide useful references for researching the failure mechanism, preventing and repairing methods for void-inducing defects of tunnel structures.

2. Experimental setup and description

2.1. Tunnel prototype description

Taking the Longxi tunnel, which was serious damaged in Wenchuan Great Earthquake, as the prototype structure. The tunnel is a 3700 m long highway tunnel connecting the towns of Dujiangyan and Yingxiu, the stretching directions of which are from southeast to northwest. The tunnel has a horseshoe shape cross section with excavated dimensions of 11.2 m width and 7.9 m height. Since Longxi tunnel is located approximately 2–3 km away from the epicenter of Wenchuan Great Earthquake and built in weak and fractured surrounding rock, rock deformation and lining crushed phenomena were very common during the construction period (Yu et al., 2016b). Moreover, Longxi tunnel is a fault-crossing tunnel below the underground water table, no wander plenty of voids were detected behind the tunnel linings especially on the lining crown.

(a)

(b)

Fig. 1. Damage modes of Longxi tunnel with voids on its crown in Wenchuan Great Earthquake 2008, China. (a) Void-inducing lining crown collapse in constructing stage; (b) Void-inducing lining crown collapse in operating period.

2.2. Shaking table array

The shaking table at Institute of Engineering Mechanics, China Earthquake Administration is a three-direction with six-degree-of-freedom shaking table array that can be excited using either electrical actuator (for high frequency shaking) or hydraulic actuator (for low frequency shaking) controlled using a digital control module (Chen et al., 2010). The digital control module allows simulation of various types of dynamic displacement time-histories, including harmonic spectrum, band limited white noise spectrum and pre-stored earthquake records. Due to the experimental requirements, the electrical actuator was used in this series research. The shaking table can efficiently run in the range of 0.5–40 Hz, the dimension of which is 5 m × 5 m in plane (see Fig. 2(a)). The maximum acceleration of shaking table is 10 m/s^2 in horizontal directions and 7 m/s^2 in vertical directions with the maximum displacement of 50 mm and maximum proof model mass of 30 tons. The accessory facilities include loading controlling devices and data logging apparatus (see Fig. 2(b) and (c)). The data logging apparatus is directly able to obtain strains, displacements and accelerations from test models during excitations.

2.3. Model container design and manufacture

A model container is fabricated and installed on the shaking table in order to contain the surrounding rock and lining models. One of the

(a)

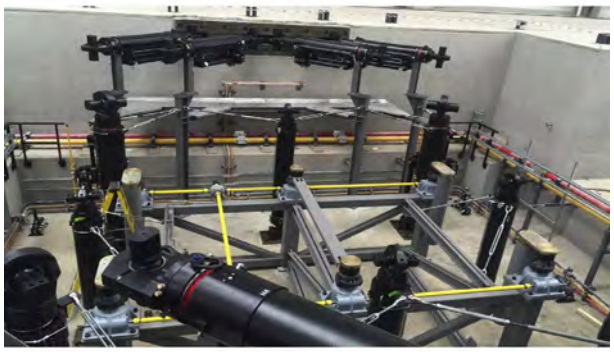

(b)

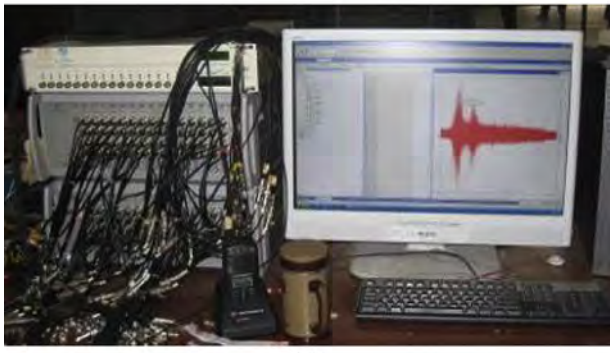

(c)

Fig. 2. Shaking table and accessory facilities. (a) Shaking table; (b) Loading controlling devices; (c) Data logging apparatus.

wide side of model container is open so that the scaled tunnel model can be put into the container and the surrounding rock can be backfilled. Further to prevent leakage of confined surrounding rock, wood sheet lining is attached to inner surface of the container. At the portal of lining model, a 50 cm wide hole is set to observe the development of earthquake-inducing cracks. Instead of welding a steel sheet on both long sides of model container, there is a Perspex sheet installed in order to observe and control tests processes conveniently (Turan et al., 2009). Fig. 3(a) shows the container, the overall dimensions of which are 3.7 m long, 1.5 m wide and 1.8 m high. Absorbing boundaries are required between the rigid surfaces and the surrounding rock to prevent the reflection and refraction of seismic waves during excitation. Polystyrene foam and polyethylene membrane are attached to inner wide and long sides of model container respectively in order to mitigate the boundary effect on the lining models (see Fig. 3(b)). Therefore, data logging apparatus is able to achieve reliable data from lining models and surrounding rock as desired during seismic excitations without much interference from the boundary regions. A layer of cement mortar is paved on the inner bottom surface in order to prevent relative slip of

(a)

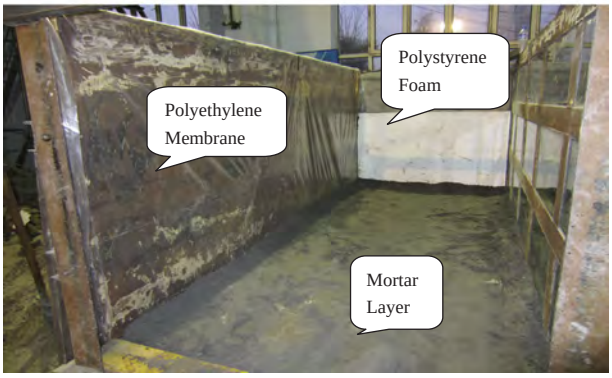

(b)

Fig. 3. Model container. (a) Model container with observation system; (b) Boundary effect mitigation measures for model container.

surrounding rock and model container. Finally, the model container is bolted firmly on the shaking table using a total of 10 bolts of high shearing strength with additional weights.

2.4. Similarity relationship and parameters

The similarity relations between prototype and model is derived based on law of similarity for shaking table model test in underground engineering (Zheng et al, 2005). Some necessary similar parameters should be satisfied. The similarity ratio of gravity acceleration C_A should be 1 since the prototype and model are in the same gravitational field. The similarity ratio of strain $C\varepsilon$ should be 1 to guarantee the seismic responses and damage of prototype and model are identical. Depending on the maximum load capacity of shaking table and the overall dimensions of model container, considering the cross section shape of tunnel prototype, a model scale of 1:25 was adopted in this series shaking table tests. Meanwhile, similarity ratio of geometry C_L, density C_ρ and Young's modulus C_E are the fundamental physical variables of shaking table tests, which can derive other physical variables. The three fundamental controlling factors of model tests should satisfy Eq. (1).

$$C_E C\varepsilon = C_L C_\rho \tag{1}$$

The similarity ratios of the tests are listed in Table 1, where physical variables with subscript p are used to describe the prototype, while physical variables with subscript m are used for the model (Sun et al., 2011). In the similarity ratios, acceleration and time are used to simulate parameters of seismic waves, while the others are used to simulate rock and lining material. However, void model material was not taken into account to satisfy the similitude relations since the function of plastic basin was to form the void model and maintain the integrity of void model during excitations.

Table 1
Similarity rules for shaking table tests.

Name	Geometry $C_L = L_p/L_m$	Young's modulus $C_E = E_p/E_m$	Density $C\rho = \rho_p/\rho_m$	Cohesive strength $C_C = C_p/C_m$	Friction angle φ (°)	Acceleration $C_A = A_p/A_m$	Time $C_t = t_p/t_m$
Similarity ratio	25	32.5	1.3	42	1.0	1.0	5

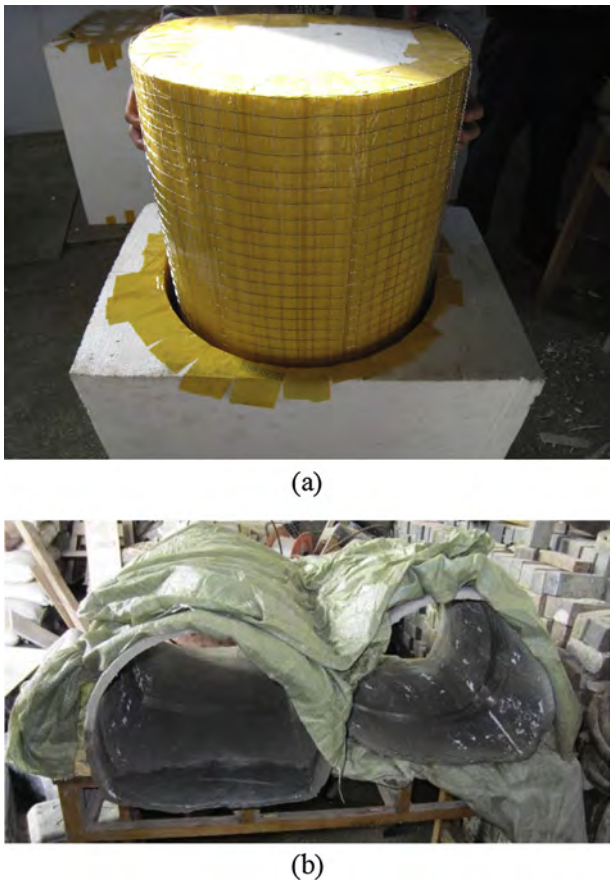

Fig. 4. Manufacturing process of tunnel models. (a) Mold and shaped steel mesh for lining model; (b) Water-cured micro-concrete lining models.

2.5. Tunnel model and surrounding rock material

The micro-concrete and shaped steel mesh were applied to simulate the tunnel lining and rebar respectively so that the tunnel model would not totally collapse because it was necessary to observe the damage progressive states and record the final damage modes (Ha et al., 2008). Besides, compared with the ordinary concrete, micro-concrete has more reasonable gradations and mechanical properties to meet the similarity rules of this series shaking table tests. Fig. 4 illustrates the manufacturing process of lining models. Each segment length of lining model is 80 cm with the thickness of 1.8 cm. According to a series of material mechanical property tests, the ultimate strains of micro-concrete material in tension and compression conditions are confirmed as 300με and 600με respectively.

Generally, surrounding rock material in shaking table tests should consist of aggregate, cement and accessory materials, then the mixture of river sand, engine oil and fly ash was used to simulate rock model because the real surrounding rock properties do not satisfy the similitude relation of this test as expected. A series of orthogonal and error dynamic tri-axial tests were conducted to find the optimal mixture content of the surrounding rock material. The mixture with mass content 57:31:12 (57 for fly ash, 31 for river sand and 12 for engine oil) provided the best match with the similitude relation. Before excitation,

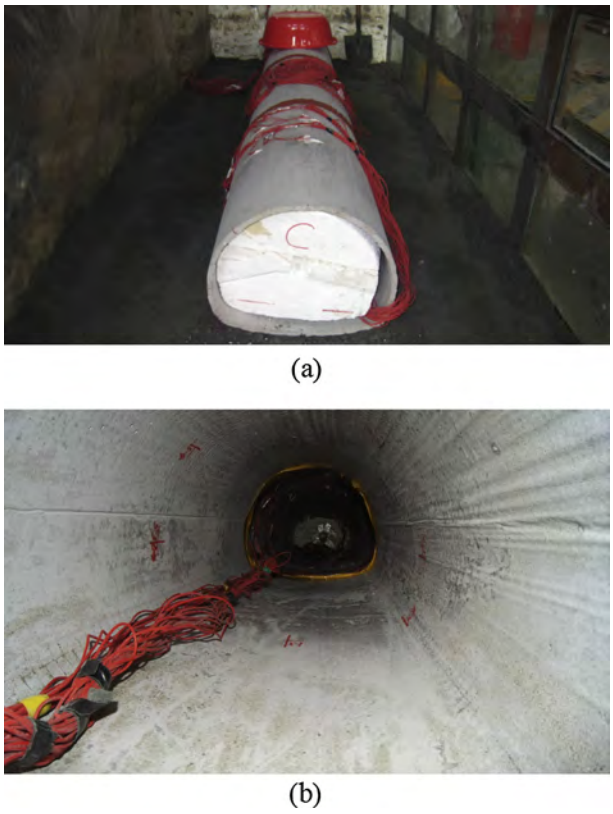

Fig. 5. Surrounding rock, void and tunnel lining model. (a) Tunnel lining and void models; (b) Inner surface of tunnel lining model.

surrounding rock material was placed into the model container layer by layer. Each layer was tamped to guarantee the consistent material density and the thickness was about 10 cm so that the material would not be bubbled (Chen et al., 2012). After complete backfilling and before the excitation, it took 7 or 8 h to wait for the settlement and compaction of surrounding rock material. According to the previous studies, a plastic basin with a diameter of 40 cm was placed as a void on lining crown to simulate the most adverse condition, which covered spandrels as well (see Fig. 5). Therefore, the void in surrounding rock was too stable to collapse during excitations so that we could describe the cracks propagation directions of lining models (Xiao, et al, 2014). Table 2 lists the material parameters used in the series shaking table tests.

3. Test schemes and instrumentation

3.1. Test schemes

The Wolong seismic waves recorded from Wenchuan Great Earthquake, which had N-S, E-W and U-D three components, directly struck the tunnel prototype and led to destruction. Thus, whereas the positions of tunnel prototype and epicenter, besides the experimental purposes, taking the E-W and U-D components as the shaking table input motions, which are constructed and adopted in Fig. 6 according to the similarity rules. Considering the void is on the crown of lining model, both E-W and U-D components are applied as horizontal and

Table 2
Surrounding rock and lining structure parameters of the model and prototype.

Name	Cohesive strength c (kPa)	Friction angle φ (°)	Young's modulus E (MPa)	Density ρ (g/cm^3)	Poisson's ratio μ	Compression strength σ (MPa)
Rock prototype	50–200	20–27	1.3e3-6e3	1.7–2.0	–	–
Rock model	1.19–4.76	20–27	40–185	1.21–1.43	–	–
Lining prototype	–	–	28e3	2.5	0.2	12.5
Lining model	–	–	980	1.94	0.2	0.3

vertical excitations respectively, which means the shaking table moves in the directions that are perpendicular to the longitudinal axis of the lining model (Sim et al., 2012). The test results from both excitation directions are discussed in this paper.

The reliability of shaking table tests data is partially dependent upon the conditions of data logging apparatus to reproduce simulated and recorded signals in excitation process (Jiang et al., 2010). Therefore, after backfilling the rock material and before changing the excitation directions, the shaking table was tuned to a group of motions scaled to the new levels. There are three static tests thereby listed in table 3, which divides the whole tests processes into two stages. Each stage has a series of seismic damage tests with increasing intensity, which are conducted by applying the same seismic signals with the same durations but multiplied by an increasing factor. Thus, there are in total twelve test cases have been carried out. Correspondingly, the PGAs of shaking table excitations grow from approximately 0.1 g (where g = 9.81 m/s^2) to 1.0 g (horizontal excitation) or to 0.7 g (vertical excitation) due to the limitation of shaking table performance.

3.2. Instrumentation

Fig. 7(a) shows a typical strain-monitoring cross-section of the lining model and the instrumentation layout. In total, sixteen strain gauges (S1–S16) are installed on both outer and inner surfaces to monitor the seismic strain responses of lining model, while the number of which are in counter clockwise order. Meanwhile, the corresponding monitoring positions are named by several settled technical terms such as crown, spandrel, sidewall, arch springing and invert. A reasonable amount of strain gauges is able to guarantee the availability and accuracy of strain data (Rojhani et al., 2012).

Fig. 7(b) is a longitudinal profile, which is designed for schematically illustrating all items applied in this series shaking table tests. As the introduction of instrumentation, the letters refer to the properties of different items (e.g., letters A, T and V mean accelerometer, cross-sections in tight contact state and cross-sections under void respectively while B, C and D are signs of different lining models). Lining models, surrounding rock and shaking table are instrumented with six accelerometers and five cross-sections of strain gauges in total. Accelerometers A1, A2 and A3 are utilized to record the time-histories curves of shaking table, model container boundary and surrounding rock interior respectively, thereby the data from them can be testified the boundary effect of container. Accelerometers A4, A5 and A6 are placed at the middle of lining crown, while A5 is covered by void, to study the difference of seismic responses from lining models with and without a void. Strain gauges around V1, V2 and V3 cross-sections are pasted under the void to record the progressive damage states of lining model while the T2 and T3 are used to research the seismic responses of lining model in tight contact states.

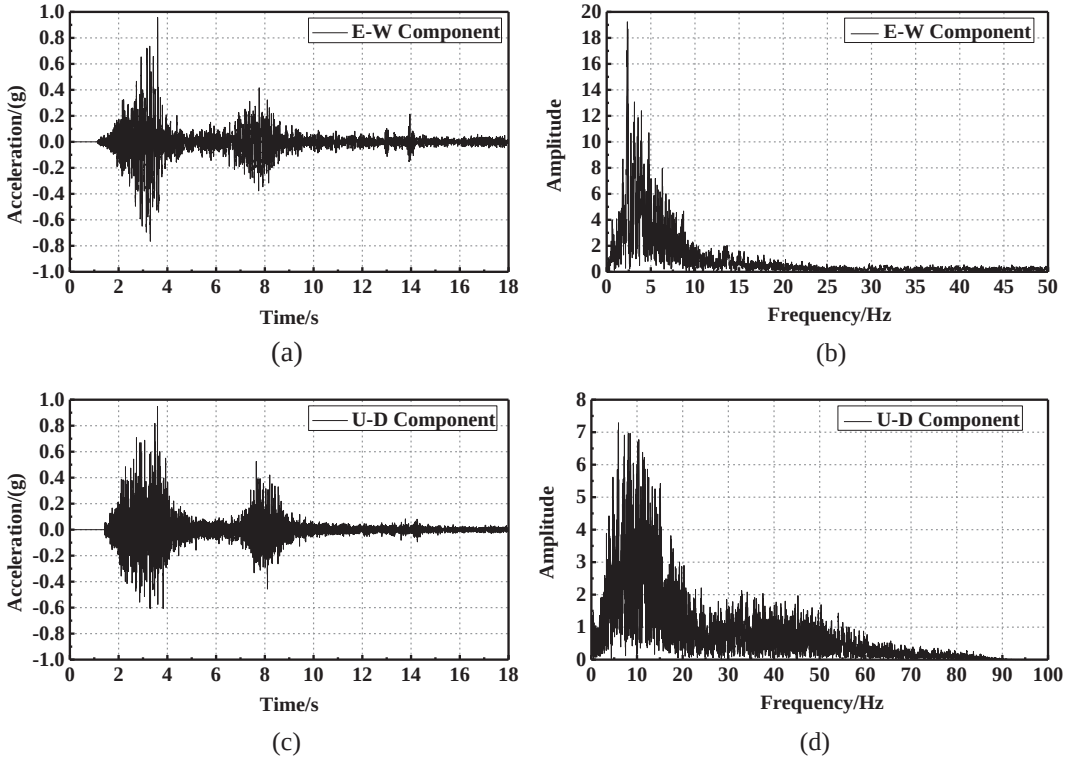

Fig. 6. Wolong seismic waves from Wenchuan Great Earthquake. (a) Acceleration time history of E-W component; (b) Fourier spectrum of E-W component; (c) Acceleration time history of U-D component; (d) Fourier spectrum of U-D component.

Table 3
Detailed information of tests schemes and input motions.

Stage ID	Test ID	Input motion	Amplitude (g)	Duration
Stage 1	Test 1	Static load	–	7–8 h
	Test 2	Wolong (E-W)	0.2	18 s
	Test 3	Wolong (E-W)	0.4	18 s
	Test 4	Wolong (E-W)	0.6	18 s
	Test 5	Wolong (E-W)	0.8	18 s
	Test 6	Wolong (E-W)	1.0	18 s
Stage 2	Test 7	Static load	–	Depending on the final balanced condition
	Test 8	Wolong (U-D)	0.2	18
	Test 9	Wolong (U-D)	0.4	18
	Test 10	Wolong (U-D)	0.6	18
	Test 11	Wolong (U-D)	0.7	18
	Test 12	Static load	–	Depending on the final balanced condition

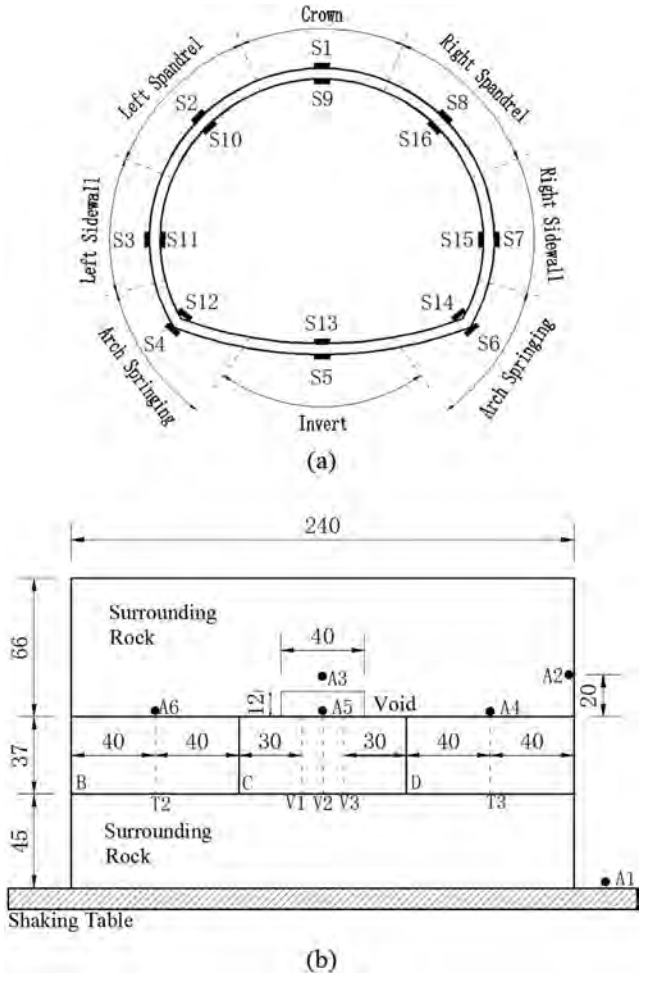

Fig. 7. Instrumentation for shaking table tests. (a) Cross section for strain gauges layout; (b) Longitudinal profile of test schemes (Unit: cm).

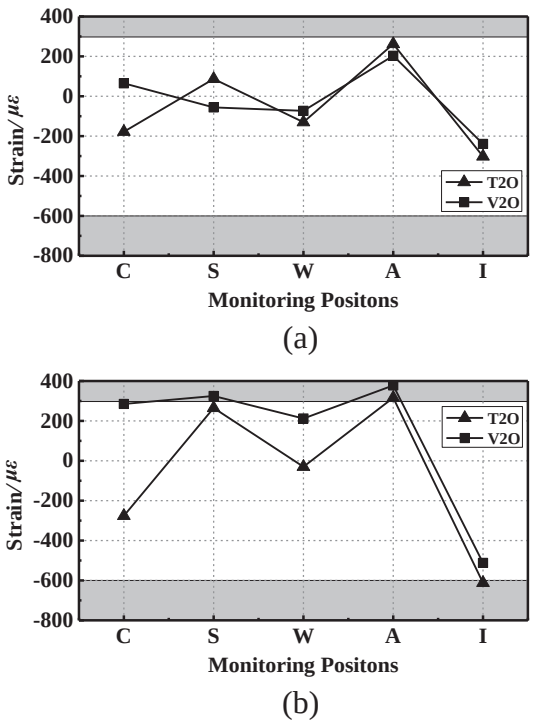

Fig. 8. Static strains in tests (the monitoring position letters C, S, W, A and I stand for crown, spandrel, sidewall, arch springing and invert respectively). (a) Strains at monitoring positions in test 1; (b) Strains at monitoring positions in test 7.

4. Test results and discussions

4.1. Static states responses

The static strains of monitoring point are obtained in test 1 and test 7. Letters in legends of Fig. 8 such as T, V and O stand for tight contact state, voids and outer surface respectively. The positive and negative values are used to define the tension and compression strains respectively. If the strain values in the top or bottom shadows of Fig. 8, it means that the monitoring points have been in drawing cracking or compression collapse states respectively. As for the micro-concrete material, it deems that the tension strain or stress are more adverse than compression ones, thus more analyses focus on data or damage phenomena about tension.

Before excitation, it is reasonable that compression strains are dominant in both tight and void states due to the horseshoe cross-section. Obviously, void cannot directly cause adverse stain conditions or even damage. In contrast, the existence of void is beneficial for reducing the absolute values of strains at all monitoring points. Additionally, except arch springing, almost all tension and compression strain values at monitoring points are quite lower than critical values of damage. It is noted that the void exchanges the tension and compression states of crown and spandrel so that the crown tends to be more vulnerable in seismic state. After horizontal excitations, spandrel and arch springing in void state have already cracked by tension stress while the strain value of crown is quite close to damage extreme. It is apparent that lining model with a void is easier to destroy by horizontal excitation. Therefore, without the counterforces of surrounding rock, the existence of void changes the pressure distribution of surrounding

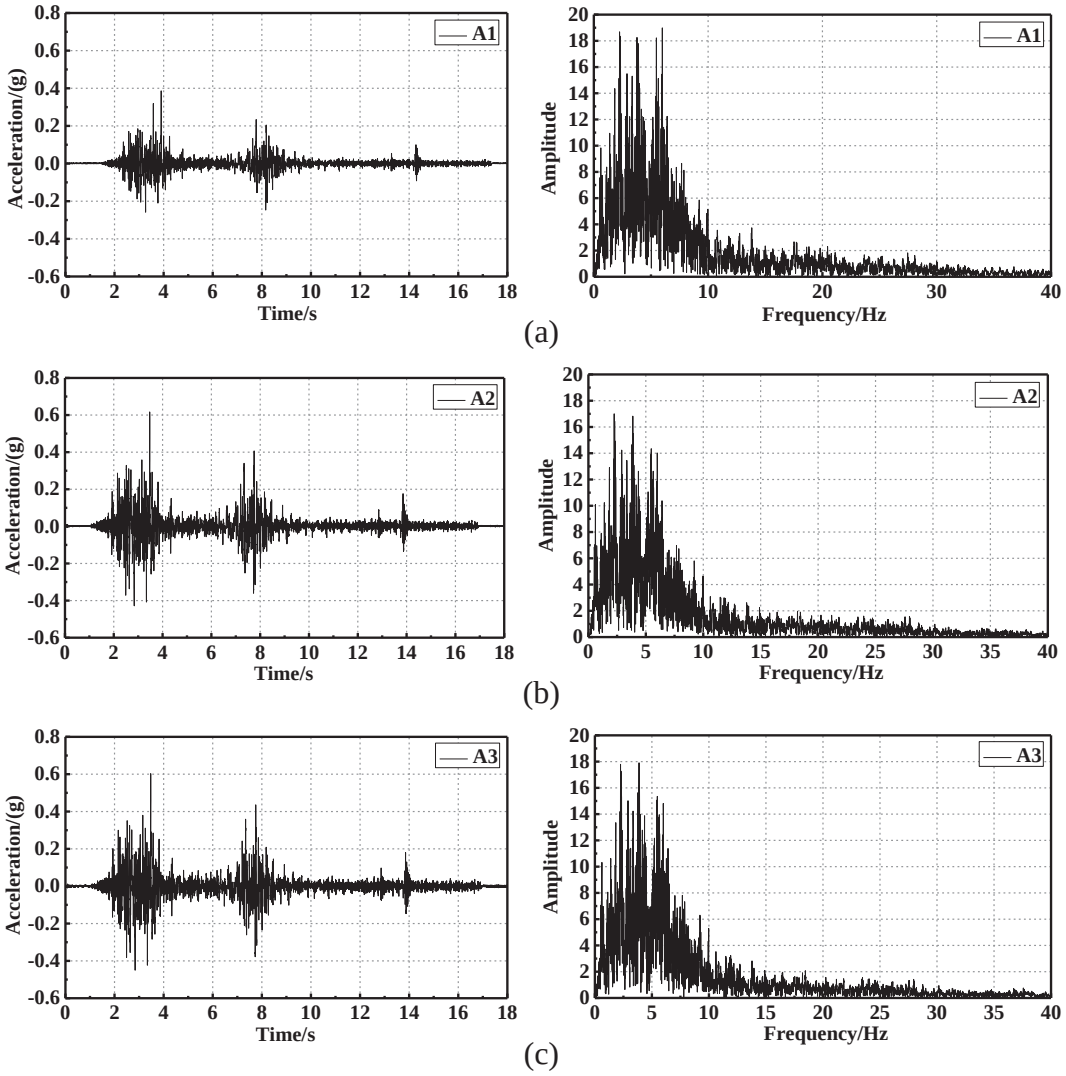

Fig. 9. Acceleration-time histories and its corresponding Fourier spectrum. (a) Acceleration-time histories and Fourier spectrum from A1; (b) Acceleration-time histories and Fourier spectrum from A2; (c) Acceleration-time histories and Fourier spectrum from A3.

rock and stress condition of supporting structures. Besides, the influence range is limited in the void-covering areas in spite of the significant effects, since the strain values at arch springing and invert are quite close to each other.

4.2. Assessment of boundary effects

Fig. 9 shows the acceleration time-histories curves and the corresponding Fourier spectrums obtained on the shaking table (A1) and at a height of 1020 mm (A2 and A3) in the container. The maximum absolute acceleration values of A1, A2 and A3 are 0.39, 0.61 and 0.60 respectively. Comparing the acceleration traces from A1 and A2 or A1 and A3, the input accelerations are amplified from the shaking tabletop to the middle of the model container because of the site response. Moreover, the differences of acceleration time histories curves and Fourier spectrums between the responses at A2 and A3 are quite insignificant. These results demonstrate that the absorbing boundaries indeed prevent seismic interference while the reflection and refraction of seismic waves from lateral boundaries can be neglected.

4.3. Acceleration response

The amplification factors are the ratios of two particular peak acceleration values, which are usually applied to reflect the dynamic response intensity instead of time-histories curves and corresponding Fourier spectrum. In this paper, we define the amplification factors as the ratios of maximum absolute acceleration values of accelerometers at monitoring points to that of accelerometer on the shaking table in each testing condition.

Fig. 10 indicates the relationships between amplification factor and the growing input PGAs with horizontal and vertical excitations while the A4 and A5 accelerometers are in tight contact and void condition respectively. It is worthwhile to note the changes around 0.4 g input PGA regardless of the excitation directions. Comparing the tight contact state, void is effectively in reducing the acceleration response of lining crown with inputting the 0.2 g or 0.4 g PGA. In contrast, with the PGAs increasing from 0.6 g to 1.0 g, the existence of void is highly effective in amplifying the seismic response of crown. This series data implies that the void-inducing damage effects will be more significant from moderate to severe earthquakes.

The surrounding rock material tends to be more solid to restrain the deformation of lining crown because of the settlement after twice excitations, which is beneficial for integral stress condition of the whole lining model. However, the vibration at void-covering crown will become stronger duo to the lack of effective counterforces from surrounding rock. In reality, it is ordinary that strong earthquakes

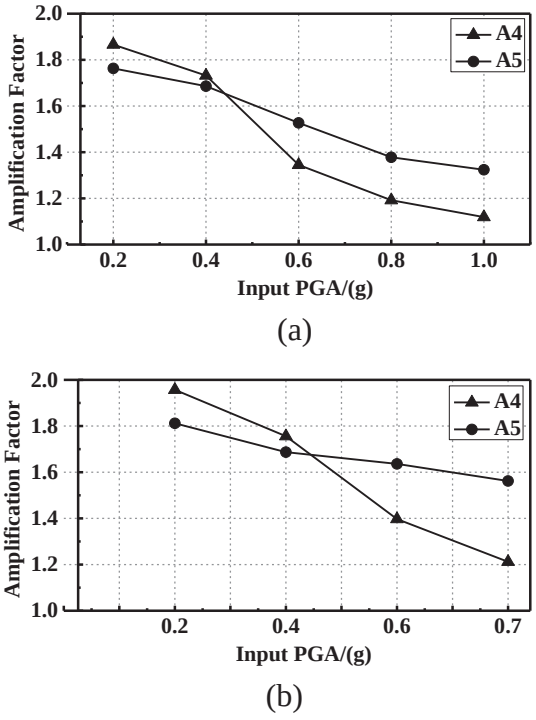

Fig. 10. Acceleration amplification factors with the increasing input PGA. (a) Accelerations responses with horizontal excitations; (b) Accelerations responses with vertical excitations.

associate with shrink and collapse of void in practical projects. Therefore, in order to avoid more severe damage, the voids should be accurately detected, effectively backfilled and grouted in constructing and operating periods.

4.4. Strain response

Tension strains are recorded and applied to analyze seismic responses of monitoring positions, since the dominant tension strains decide the diverse damage states of lining models due to the micro-concrete material. As mentioned previously, the ultimate tensile strain value of micro-concrete is 300 με, thus in Fig. 11, data in shadow areas means that the corresponding positions have cracked. Due to the significant effect of horizontal excitation on lining model with a void, all monitoring positions cracked before vertical excitation. Therefore, there are three sub-diagrams in Fig. 11 instead of four.

As presented in Fig. 11, horizontal excitation is highly effective in increasing seismic strain responses at spandrel and arch springing. Besides, the cracks at arch springing also attribute to stress concentration due to horseshoe cross-section regardless of seismic and void effects, but the excitation is beneficial for amplifying negative effect of void indeed. Moreover, crown should be the vulnerable position as well due to the void-inducing adverse stress condition. It is noteworthy that horizontal excitation and void hardly affect the sidewall. Almost all monitoring positions are damaged with 0.6 g input PGA due to the combined effects of seismic and void. However, all the monitoring positions of cross-section without void are in reasonable strain conditions with the increasing PGA at 0.2 g and 0.4 g. It is obvious that the existence of void reduces the aseismic capacity and changes the damage mode of lining model due to the lack of counterforces from surrounding rock. Although the vertical excitation does not significantly affect the damaged positions such as spandrel, sidewall and arch springing any more, it triggers the destruction of crown and invert and increases tension strain values at all monitoring positions.

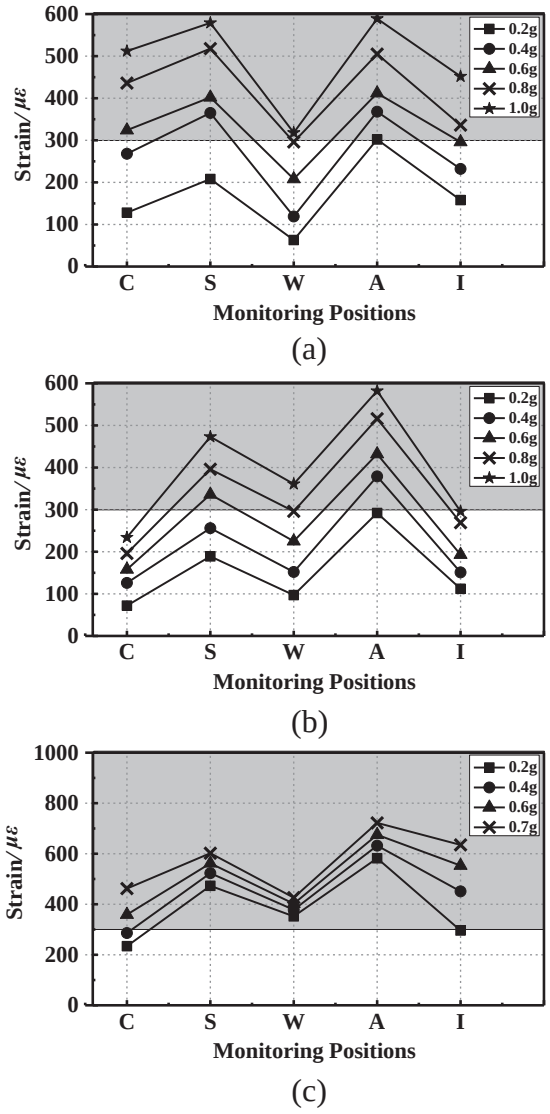

Fig. 11. Seismic strain response of monitoring positions. (a) Seismic strain responses of lining model with void (horizontal excitation); (b) Seismic strain responses of lining model without void (horizontal excitation); (c) Seismic strain responses of lining model without void (vertical excitation).

4.5. General observation

Since each excitation can lead to varying degrees destruction of lining model, each damage state of lining is inspected by cameras and camcorders after changing input PGAs. Besides, the damage condition of each monitoring point is recorded in Table.4. The arch springing is the first damage point regardless of the existence of void, since the stress concentration usually happens at arch springing. Then, the next damage position is spandrel. According to the previous research, the horizontal excitation is generally related to the 45° isogonal conjugate deformation of lining cross section, thereby the spandrel and arch springing would be the most vulnerable positions. The lining model in tight contact state has a better aseismic performance in horizontal excitation stage, since only three monitoring position except crown and invert are damaged while all the monitoring positions of void-covering lining model are damaged. It is obvious that the combined effect of seismic and void is effective in worsening the stress and deformation conditions of lining model.

However, the lining model in tight contact state cannot withstand the vertical excitations because the invert and crown are damaged at

Table 4
Progressive damage states of lining models.

Lining models	Monitoring points	Horizontal excitations					Vertical excitations			
		0.2 g	0.4 g	0.6 g	0.8 g	1.0 g	0.2 g	0.4 g	0.6 g	0.7 g
With void	Crown			×	×	×	×	×	×	×
	Spandrel		×	×	×	×	×	×	×	×
	Sidewall					×	×	×	×	×
	Arch springing	×	×	×	×	×	×	×	×	×
	Invert				×	×	×	×	×	×
Without void	Crown								×	×
	Spandrel			×	×	×	×	×	×	×
	Sidewall					×	×	×	×	×
	Arch springing		×	×	×	×	×	×	×	×
	Invert						×	×	×	×

0.2 g and 0.6 g respectively. Generally, the invert is subjected to large bending moment while the vertical excitation triggers the moment-inducing damage at invert. The tight contact state above the crown is quite reasonable, since the crown is the last damage position. Whereas the progressive damage states of lining model cannot be easily analyzed in vertical excitation stage due to the vulnerability, thus, the final damage patterns of lining should be concerned.

After completing the excitations, lining models were dug out from surrounding rock material, the cracks on which were distinguished and described by red maker pens. As shown in Fig. 12, both the outer and inner surfaces of lining with a void are more serious damaged than the lining model without a void. It is obvious that there are three drawing annular cracks on the outer surface of crown, besides, longitudinal cracks spread from spandrel to invert on both outer and inner surfaces. These phenomena illustrate the deformation tendency of crown and verify the preceding analyses in this paper. However, there are only longitudinal cracks rather than annular ones on the surfaces of lining model without a void while the spandrel, arch springing and invert are considered as the vulnerable positions.

The roof collapse did not happen in surrounding rock in spite of the existence of void, but a 2 cm settlement of rock was observed after excitations.

5. Summary and conclusions

By means of comparative shaking table tests, the earthquake-inducing damage patterns of tunnel lining with and without a void on the crown are clarified. Since the effect of void contains a certain influence range on tunnel lining, the correlation between tunnel lining and void is researched in this paper. The following is a summary of the results and conclusions arising from this study:

1. In static state, the tight contact state of lining and rock is highly effective in maintaining stability of tunnels because lining structures sustain uniform loads from surrounding rock and produce sufficient counterforces. Conversely, the existence of void changes pressure distribution law of surrounding rock and stress condition of lining structures. The bending moment at lining crown will increase while

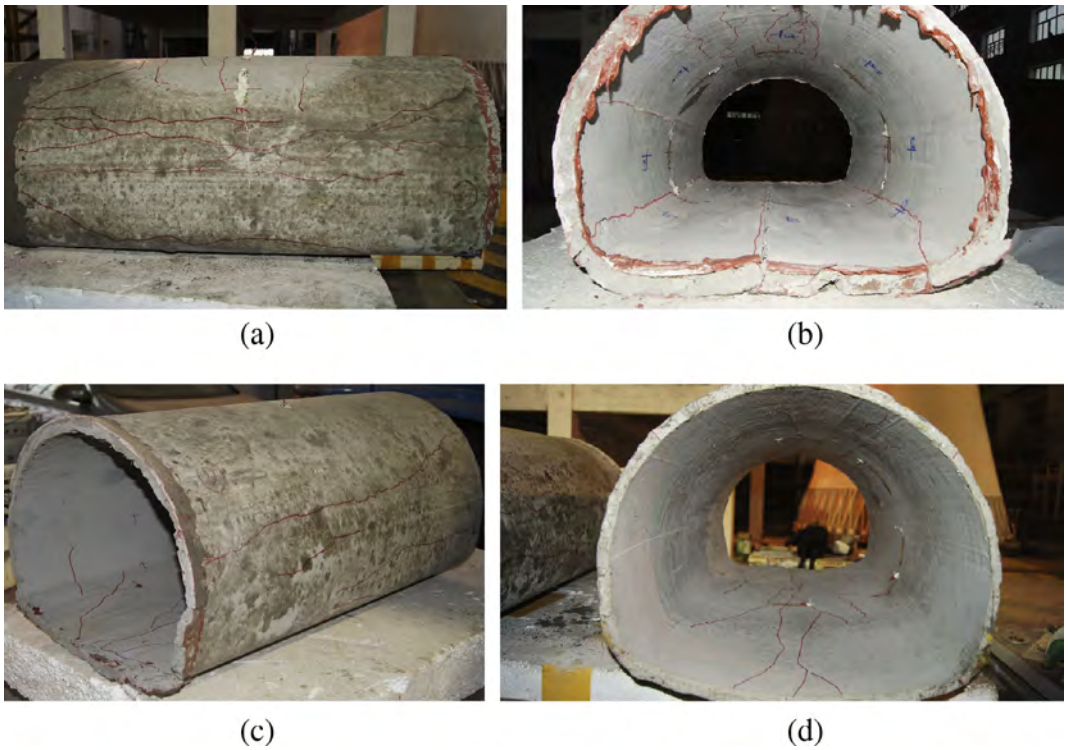

Fig. 12. Cracks on outer and inner surfaces of lining models. (a) Cracks on outer surface of lining model with void; (b) Cracks on inner surface of lining model with void; (c) Cracks on outer surface of lining model without void; (d) Cracks on inner surface of lining model without void.

the axial force will decrease due to the lack of vertical resisting forces and plenty of horizontal expansion forces from surrounding rock. Thus, lining structures will be easy to crack by tensile stress, which will directly result in the reduction of carrying capacity and security of tunnel structures.

2. In static state, the discontinuity point-contact of void and lining causes the stress concentration, which is related to the compression and tension strains on the inner and outer surfaces of lining crown respectively. Then the tensile stress contributes to annular cracks or even bulge deformation of lining structures. Besides, it causes strain mutation zone and affects the stableness along the longitudinal direction of lining and rock, though it will be unlikely to destroy the lining structures.
3. In seismic state, although the strain values of lining structures in tight contact state are little higher, it will not generate severe damage. Oppositely, the void can significantly diminish strains, peak acceleration and relative deformation of lining model when the input PGAs are at 0.2 g and 0.4 g. However, the strain and acceleration responses of lining will become significant with the growing PGA beyond 0.4 g. Therefore, the existence of void on the crown reduces the aseismic capacity and changes the damage modes of tunnel structures.
4. In seismic state, there is no doubt that the strongest seismic responses occur at lining crown. Accordingly, besides the excitation, void contributes to the strain amplification at crown, which is deemed as the main inducement of lining cracks. Thus, the excitation promotes the negative effects of voids. However, the existence of void does not change seismic response features of other monitoring positions, while the excitation does not enlarge the influence range of void as well. Additionally, the cyclic deformation of lining model caused by excitation should not be neglected, since it may be associated with more severe damage.
5. In seismic state, unexpected high tension strains and annular cracks occur at the outer surface of lining crown and spandrel mainly due to the vertical excitation. Although lining models do not collapse due to the existence of shaped steel mesh, the damage modes of lining model with and without void are quite similar with corresponding ones in tunnel prototype. In contrast, tunnel prototype without rebar cannot effectively limit strain values and prevent collapse. At last, arch springing and invert of lining model with avoid are also severely damaged due to the lack of integrity.

Acknowledgements

The National Natural Science Foundation of China (Grant No. 51604183 & 51778109) supported this research. All supports are gratefully acknowledged.

References

Balkaya, M., Moore, I.D., Sağlamer, A., 2012. Study of non-uniform bedding due to voids under jointed PVC water distribution pipes. Geotext. Geomembr. 34, 39–50.
Baziar, M.H., Moghadam, M.R., Kim, D.S., et al., 2014. Effect of underground tunnel on the ground surface acceleration. Tunn. Undergr. Space Technol. 44, 10–22.
Chen, J., Jiang, L.Z., Li, J., et al., 2012. Numerical simulation of shaking table test on utility tunnel under non-uniform earthquake excitation. Tunn. Undergr. Space Technol. 30, 205–216.
Chen, J., Shi, XJ., Li, J., 2010. Shaking table test of utility tunnel under non-uniform earthquake wave excitation. Soil Dyn. Earthq. Eng. 30 (11), 1400–1416.
Fang, Y., Guo, J.N., Kang, H.B., et al., 2016. Influence of voids behind lining on the mechanical behavior of lining structure of highway tunnel in watery strata. Chin. J. Rock Mech. Eng. 35 (8), 1648–1658.
Fraldi, M., Guarracino, F., 2009. Limit analysis of collapse mechanisms in cavities and tunnels according to the Hoek-Brown failure criterion. Int. J. Rock Mech. Min. Sci. 46 (4), 665–673.
Gao, Y., Jiang, Y.J., Li, B., 2014. Estimation of effect of voids on frequency response of mountain tunnel lining based on microtremor method. Tunn. Undergr. Space Technol. 42, 184–194.
Ha, D., Abdoun, T.H., O'Rourke, M.J., et al., 2008. Centrifuge modeling of earthquake effects on buried high-density polyethylene (HDPE) pipelines crossing fault zones. J. Geotech. Geoenviron. Eng. 134 (10), 1501–1515.
Huang, F., Zhu, H.H., Xu, Q.W., et al., 2013. The effect of weak interlayer on the failure pattern of rock mass around tunnel-scaled model tests and numerical analysis. Tunn. Undergr. Space Technol. 35, 207–218.
Jiang, L.Z., Chen, J., Li, J., 2010. Seismic response of underground utility tunnels: shaking table testing and FEM analysis. Earthq. Eng. Eng. Vib. 9 (4), 555–567.
Jones, S., Hunt, H., 2011. Voids at the tunnel soil-interface for calculation of ground vibration from underground railways. J. Sound Vib. 330 (2), 245–270.
Leung, C., Meguid, M.A., 2011. An experimental study of the effect of local contact loss on the earth pressure distribution on existing tunnel linings. Tunn. Undergr. Space Technol. 26 (1), 139–145.
Li, T.B., 2012. Damage to mountain tunnels related to the Wenchuan earthquake and some suggestions for aseismic tunnel construction. Bull. Eng. Geol. Environ. 71 (2), 297–308.
Meguid, M.A., Dang, H.K., 2009. The effect of erosion voids on existing tunnel linings. Tunn. Undergr. Space Technol. 24 (3), 278–286.
Moghadam, M.R., Baziar, M.H., 2016. Seismic ground motion amplification pattern induced by a subway tunnel: shaking table testing and numerical simulation. Soil Dyn. Earthq. Eng. 83, 81–97.
Nie, Z.Y., Zhang, C.L., Li, F.X., 2015. Effect of void behind lining on seismic performance of tunnel. China Earthq. Eng. J. 37 (1), 138–143.
Oreste, P., 2014. The determination of the tunnel structure loads through the analysis of the interaction between the void and the support using the convergence-confinement method. Am. J. Appl. Sci. 11 (11), 1945–1954.
Rojhani, M., Moradi, M., Galandarzadeh, A., et al., 2012. Centrifuge modeling of buried continuous pipelines subjected to reverse faulting. Can. Geotech. J. 49 (6), 659–670.
Sim, W.W., Towhata, I., Yamada, S., et al., 2012. Shaking table tests modelling small diameter pipes crossing a vertical fault. Soil Dyn. Earthq. Eng. 35, 59–71.
Sun, T.C., Yue, Z.R., Gao, B., et al., 2011. Model test study on the dynamic response of the portal section of two parallel tunnels in a seismically active area. Tunn. Undergr. Space Technol. 26, 391–397.
Turan, A., Hinchberger, S.D., El Naggar, H., 2009. Design and commissioning of a laminar soil container for use on small shaking table. Soil Dyn. Earthq. Eng. 29, 404–414.
Wang, J.F., Huang, H.W., Xie, X.Y., et al., 2014. Void-induced liner deformation and stress redistribution. Tunn. Undergr. Space Technol. 40, 263–276.
Wang, J.F., Huang, H.W., Xie, X.Y., et al., 2010. Risk assessment of voids behind the lining of mountain tunnels. Geo Florida 2010: advances in analysis. Model. Design Conf. 2010, 2319–2328.
Wang, W.L., Wang, T.T., Su, J.J., et al., 2001. Assessment of damage in mountain tunnels due to the Taiwan Chi-Chi earthquake. Tunn. Undergr. Space Technol. 16 (3), 133–150.
Wang, Z.Z., Gao, B., Jiang, Y.J., et al., 2009. Investigation and assessment on mountain tunnels and geotechnical damage after the Wenchuan earthquake. Sci. China Ser. E: Technol. Sci. 52 (2), 546–558.
Wang, Z.Z., Jiang, Y.J., Zhu, C.A., et al., 2015. Shaking table tests of tunnel linings in progressive states of damage. Tunn. Undergr. Space Technol. 50, 109–117.
Wang, Z.Z., Zhang, Z., 2013. Seismic damage classification and risk assessment of mountain tunnels with a validation for the 2008 Wenchuan earthquake. Soil Dyn. Earthq. Eng. 45, 45–55.
Xiao, J.Z., Dai, F.C., Wei, Y.C., et al., 2014. Cracking mechanism of secondary lining for a shallow and asymmetrically-loaded tunnel in loose deposits. Tunn. Undergr. Space Technol. 43, 232–240.
Yu, H.S., Rowe, R.K., 1999. Plasticity solutions for soil behavior around contracting cavities and tunnels. Int. J. Numer. Anal. Meth. Geomech. 23, 1245–1279.
Yu., H.T., Cai, C., Guan, X.F., et al., 2016a. Analytical solution for long lined tunnels subjected to travelling loads. Tunn. Undergr. Space Technol. 58, 209–215.
Yu, H.T., Chen, J.H., Bobet, A., et al., 2016b. Damage observation and assessment of the Longxi tunnel during the Wenchuan earthquake. Tunn. Undergr. Space Technol. 54, 102–116.
Zhang, C.P., Zhang, X., Li, H., et al., 2016. Model tests on failure laws of ground with voids induced by shallow tunnelling. Chin. J. Geotech. Eng. 38 (2), 263–270.
Zhang, D.L., Zhang, S.L., Fang, Q., et al., 2013. Study of contact state behind tunnel lining in process of railway operation and its analysis. Chin. J. Rock Mech. Eng. 32 (2), 217–224.
Zheng, Y.L., Yang, L.D., Li, W.Y., et al., 2005. Earthquake Resistance Of Underground Engineering. Tongji University Press, Shanghai.
Zhou, J.F., Qin, C.B., Chian, S.C., et al., 2017. Determination of critical distance for deep tunnels with a longitudinal water-filled cavity positioned above tunnel roof. Int. J. Rock Mech. Min. Sci. 93, 115–123.